Algorithm Theoretical Basis Document (ATBD)
for
Deep Convective Cloud (DCC) method of inter-calibrating geostationary imagers with a polar-orbiting reference instrument

Prepared by:
Version:
Date:

List of figures

List of Tables

Table of Contents

1. Introduction

Deep convective clouds (DCC) are the brightest and coldest natural invariant targets over the tropics suitable for vicarious calibration of satellite imagers in the reflective solar spectrum. Because they are located near tropopause height, the impact of water vapor absorption is much smaller compared to that of the ground targets. DCC also offer the highest signal-to-noise ratio (SNR) and have nearly Lambertian reflectance spectra in the visible (VIS) and near-infrared (NIR) spectrum. Distributed globally across tropical domains, DCC are applicable for calibrating both geostationary Earth orbiting (GEO) and low-Earth orbiting (LEO) satellite sensors. The DCC invariant target (DCC-IT) calibration method is a large-ensemble statistical approach, which relies on robust sampling, rather than individually identified DCC pixels, and assumes that the distribution of DCC reflectance in the VIS and NIR spectrum remains nearly constant in time. This ATBD describes the comprehensive details of the DCC-IT and its implementation for vicarious inter-calibration of GEO and LEO satellite visible sensors.

1.1 Purpose

This ATBD was prepared by NASA's Clouds and the Earth's Radiant Energy System (CERES) imager and geostationary calibration group (IGCG) to provide guidance on the implementation of DCC-IT and promote its usage among the Global Space-Based Inter-Calibration System (GSICS) members for generating consistent inter-calibration products that are essential for accomplishing radiometric harmonization among space-based observations worldwide. It describes a DCC-IT algorithm for performing an accurate transfer of calibration between a reference LEO instrument and a target GEO imager for reflective solar bands with wavelengths less than 1 μm. It is noteworthy to mention here that the DCC-IT algorithm does not require ray-matched DCC observations between the two sensors. For on-orbit inter-calibration studies, the Aqua-MODIS sensor was the first recommended GSICS reference instrument for visible channels in late 2000's. For nearly two decades, the stable MODIS calibrated radiances have been used by GSICS Processing and Research Centers as benchmark measurements for calibrating numerous geostationary imagers that lack on-board calibrators [1] With Aqua-MODIS operating well beyond its design lifetime and near de-orbiting phase, the GSICS recommends using the NOAA-20 VIIRS as the follow-on reference instrument for reflective solar band (RSB) calibration of next generation GEO sensors. The VIIRS design was built with a strong heritage from MODIS and has the advantage of having very similar spectral response functions with the next generation GEO imagers. This ATBD describes the DCC-IT method using NOAA-20 VIIRS as a reference instrument and allows the computation of a monthly calibration slope (or cross-calibration ratio) to radiometrically scale the GEO observations to equivalent NOAA-20 VIIRS radiances.

1.2 Acronyms and notations

Δ_{PDF}	PDF bin size
θ_{Solar}	solar azimuth
θ_{Sensor}	sensor azimuth
σ_{VIS}	spatial standard deviation of visible pixels
σ_{IR}	spatial standard deviation of IR pixels
$Count_{observed}$	observed sensor pixel count
$Count_{corrected}$	anisotropy-corrected sensor pixel count
$C_{GEO,MODE,observed}$	GEO DCC mode count
$L_{observed}$	observed pixel radiance
$L_{corrected}$	anisotropy-corrected pixel radiance
$L_{GEO,MODE,reference}$	GEO reference mode radiance
$L_{VIIRS,MODE}$	reference VIIRS DCC mode radiance
$\gamma_{cal-ratio}$	GEO-VIIRS cross-calibration ratio
$\gamma_{GEO,cal-slope}$	GEO calibration slope
$Slope_0$	force-fit slope of regression
U_{Ref}	reference DCC mode uncertainty
U_{SBAF}	SBAF uncertainty
U_{RegFit}	temporal regression fit uncertainty
ABI	Advanced Baseline Imager
ADM	angular distribution model
ATBD	Algorithm Theoretical Basis Document
ATO	all-sky tropical ocean
AVHRR	Advanced Very High-Resolution Radiometer
BT	Brightness temperature
CERES	Clouds and the Earth's Radiant Energy System
DCC	deep convective clouds
DCC-IT	DCC invariant target
GEO	geostationary Earth orbiting
IR	infrared
LEO	low-Earth orbiting
LUT	look up table
MODIS	Moderate Resolution Imaging Spectroradiometer
NIR	near-infrared
PDF	probability distribution function
R	Hu anisotropy factor
RAA	relative azimuth angle
RSB	reflective solar bands
SBAF	spectral band adjustment factor
SC	space count
SI	seasonal index
SCIAMACHY	SCanning Imaging Absorption spectroMeter for Atmospheric CHartographY
SRF	spectral response function

SZA	solar zenith angle
TRMM	Tropical Rainfall Measuring Mission
VIIRS	Visible and Infrared Radiometer Suite
VIRS	Visible and Infrared Scanner
VIS	visible
VZA	view zenith angle

1.3 Referencing this document

Bhatt, R., Doelling, D. R., ….. "Algorithm Theoretical Basis Document (ATBD) for Deep Convective Cloud (DCC) method of inter-calibrating geostationary imagers with a polar-orbiting reference instrument," 2021.

2. Algorithm Description

DCC are an excellent invariant Earth target for the post-launch radiometric calibration of satellite sensors. The DCC-IT is a large-ensemble statistical approach that does not rely on any individual DCC cell. When observed collectively, DCC behave as an invariant target. The first attempt of using the collective DCC pixels as an invariant calibration target was made by Hu et al. [2] to examine the radiometric stability of the CERES shortwave measurements on board the Tropical Rainfall Measuring Mission (TRMM), as well as of the Visible and Infrared Scanner (VIRS) and Moderate Resolution Imaging Spectroradiometer (MODIS) imagers on TRMM and Terra satellites, respectively. Shortly thereafter, Doelling et al. [3] refined the technique to monitor the temporal calibration drift of the Advanced Very High Resolution Radiometer (AVHRR) sensors on board the NOAA-16 and NOAA-17 satellites [4]. A simple 11-µm IR brightness temperature (BT) threshold of 205 K was used to identify the DCC pixels over the tropics. Later, Doelling et al. [5] also characterized the dependency of the DCC narrowband albedo response upon solar and viewing geometry, the 11-µm BT threshold, and the geographic domain using the Aqua-MODIS band 1 DCC observations. It was found that the DCC response could be affected by both the BT threshold and geo-location. The DCC-IT can be used for independently monitoring a sensor stability over time as well as for performing an inter-comparison between two sensors [1], [3], [6]–[9].

This ATBD follows the same baseline DCC calibration approach as described by Doelling et al. [5] with additional refinements adapted to perform a more accurate transfer of calibration from the reference VIIRS instrument to a target GEO imager. The DCC-IT calibration technique is a multi-step process that includes identification of DCC pixels, angular, spectral, and statistical transformation of the data, and estimation of cross-calibration coefficients and temporal radiometric trends. The various steps of DCC-IT calibration are described in detail in the following sections.

2.1 Extraction of DCC data

The success of the DCC-IT technique relies on a large ensemble of identified DCC pixels. To successfully transfer the calibration from NOAA-20 Visible and Infrared Radiometer Suite (VIIRS) to a target GEO sensor, both instruments should capture the DCC pixels using similar identification thresholds. The DCC-IT identifies any tropical pixel with 11-µm BT less than 205 K as DCC. Because of slight regional dependence of DCC response, the DCC identification domain is confined to ±20° latitude and longitude from the GEO sub-satellite point. To capture only the convective core and avoid cloud edges, a spatial uniformity threshold is applied by computing the spatial standard deviation of the identified pixel and its eight surrounding neighbors. Pixels with the visible (0.65 µm) standard deviation (σ_{VIS}) < 3% and the IR BT standard deviation (σ_{BT}) < 1.0 K are used. These general thresholds were derived empirically and are applicable to most GEO and LEO satellite imagers. The DCC-IT technique, therefore, requires good IR and VIS co-registration, temporally stable IR calibration, and a visible sensor dynamic range that does not saturate at bright DCC radiances. Both visible and IR pixels must have the same spatial resolution. To take advantage of the more Lambertian part of the DCC reflectance field, solar zenith angles (SZA) and view zenith angles (VZA) are also limited to less than 40°. Furthermore, direct backward and forward scattering conditions are also eliminated from the DCC sample by restricting the relative azimuth angle (RAA) of the DCC measurements to within 10-170°. The RAA is derived using the set of equations described below:

$$\delta = \theta_{Solar} - \theta_{Sensor}$$
$$\text{If } \delta \geq 360°, \; then \; \delta = \delta - 360°$$
$$\text{If } \delta < 0, \; then \; \delta = \delta + 360°$$
$$RAA = |\delta - 180°| \qquad \text{..... (1)}$$

where, θ_{Solar} and θ_{Sensor} are the solar and sensor azimuth angles, respectively. In addition, the GEO image acquisition times are chosen to match the local equator crossing time of the reference sensor. Five GEO images surrounding the 1:30 PM local time (equator crossing time of NOAA-20) provide adequate DCC samples for DCC-IT. Figure 1 shows DCC identification domains for prime GEO locations highlighted in different color square boxes.

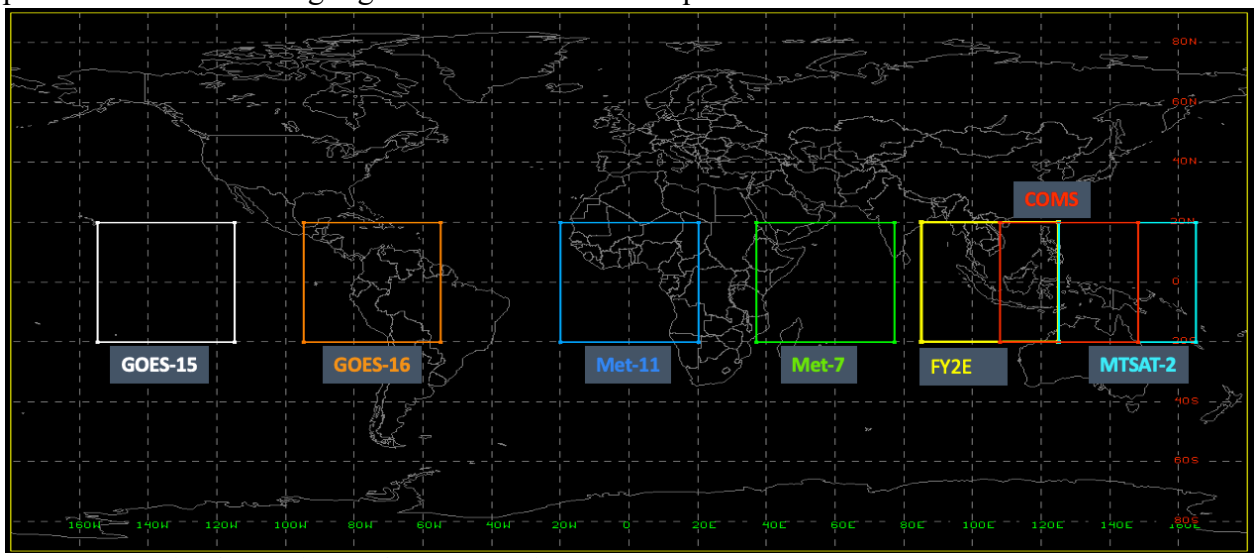

Figure 1: DCC identification domains for prime GEO locations.

2.2 11-µm BT normalization

For DCC-IT, the 11-µm BT is the key in identifying DCC pixels. Although the target GEO and the reference LEO instruments may both have onboard blackbodies for calibrating the IR channels, any difference in the spectral response functions (SRF) of the two IR channels can result in a finite radiometric bias between the corresponding BT measurements. Because the DCC-IT visible response is influenced by the BT threshold [5], [10], it is critical to normalize the GEO imager IR BT to equivalent reference LEO IR BT. The SRFs of IR channels onboard Aqua-MODIS (band 31), NOAA-20 VIIRS (band M15), GOES-16 (band 14), GOES-15 (band 4), Meteosat-11 (band 9), and Himawari-8 (Him-8) AHI imagers are shown in Figure 2a. The blackbody spectral emission at 205 K is also shown in the background. The intensity of the blackbody spectral emission increases with wavelength and peaks near 14 µm. The Aqua-MODIS and NOAA-20 VIIRS IR channels exhibit significant differences in their SRFs. The center wavelengths of the IR channels onboard the Aqua-MODIS, GOES-16 ABI, and Him-8 AHI imagers have shifted towards right compared to those onboard NOAA-20 VIIRS, GOES-15, and Meteosat-11, thereby indicating that the former three instruments measure slightly warmer BT than the latter three imagers for the same DCC pixels. If this discrepancy is not accounted for, the DCC samplings between these instruments will be biased, and the inter-calibration results will be adversely affected. An one-time BT correction term for IR channel SRF differences between a reference and a target sensor can be estimated from coincident, co-angled, and co-located BT pairs

acquired from the two instruments over all-sky tropical ocean (ATO) targets [1], [10]. Figure 2b shows the linear regression of ATO ray-matched BT pairs for NOAA-20 VIIRS M15 and GOES-16 ABI B14 from October 2019. The VIIRS and ABI BT observations are averaged on a 0.5°x0.5° grid. The presence of a non-zero offset term in the regression suggests that the spectrally induced bias in the IR measurements is a function of BT. A DCC pixel with a BT of 205 K measured by the NOAA-20 VIIRS M15 channel is recorded relatively warmer (206.3 K) by GOES-16 ABI B14. The DCC sampling and the IR BT threshold are found to have an exponential relationship. Figure 3 illustrates the monthly sample size of the DCC pixels identified globally by NOAA-20 VIIRS over the tropics (±20°latitude) for October 2018 as a function of the M15 BT threshold. A ~40% increment in the monthly DCC sample can be observed by increasing the BT threshold from 204 K to 206 K. Because adequate and consistent sampling of DCC pixels is essential for DCC-IT, the DCC identification BT threshold for the target GEO sensor must be normalized to match the equivalent VIIRS IR channel for reliable inter-calibration between the two sensor pair. In the case of GOES-16 ABI, a BT threshold of 206.3 K should be used for identifying the GEO DCC pixels over the tropical DCC domain. Table 1 provides the normalized BT threshold (equivalent to VIIRS M15 BT of 205 K) for selected GEO imagers for consistent sampling between the GEO and VIIRS sensors.

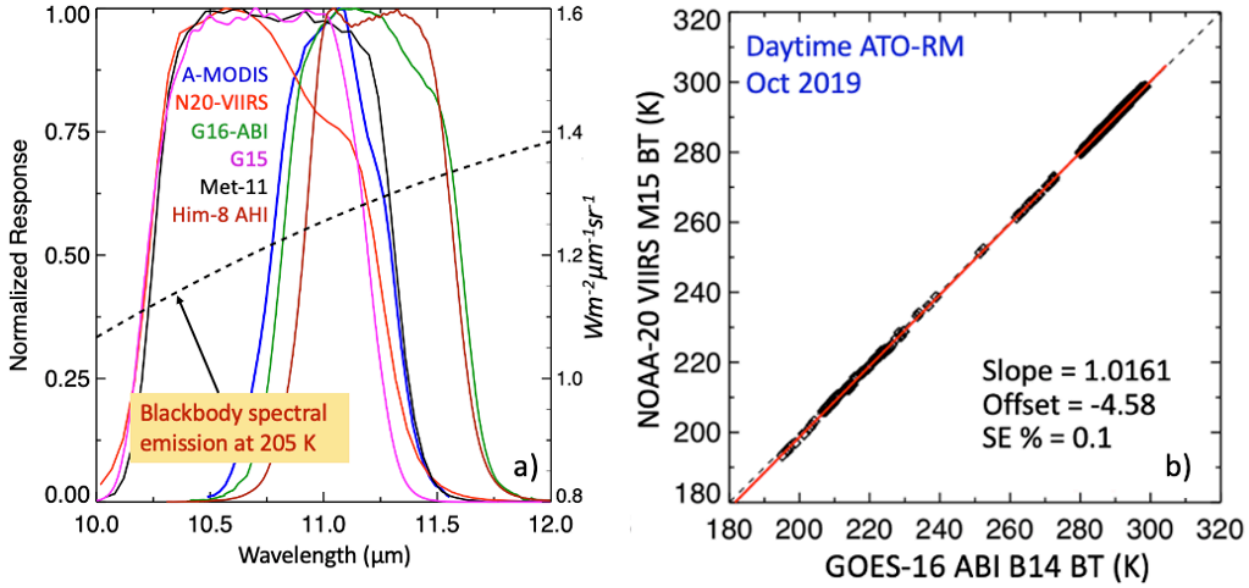

Figure 2: (a) SRF differences between Aqua-MODIS, NOAA-20 VIIRS, GOES-16 ABI, GOES-15 and Meteosat-11 IR channels. (b) Linear regression of daytime ATO ray-matched BT pairs for NOAA-20 VIIRS M15 and GOES-16 ABI B14 bands during October 2019.

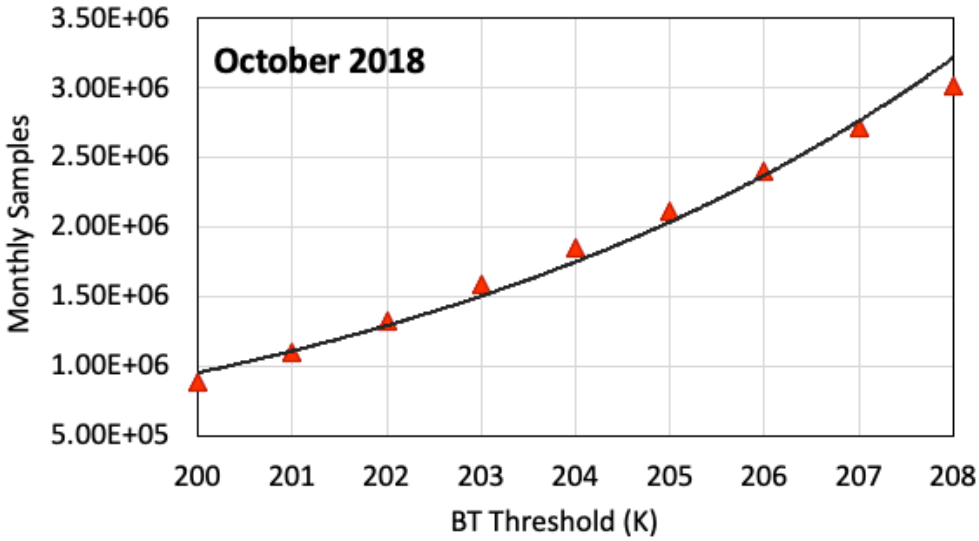

Figure 3: Number of DCC pixels identified globally within ±20°latitude by NOAA-20 VIIRS for October 2018 as a function of the M15 BT threshold.

Table 1: GEO BT thresholds (equivalent to NOAA-20 VIIRS M15 band BT of 205 K) for identifying DCC pixels over the GEO domains.

GEO Imager IR Channel	*BT threshold equivalent to VIIRS M15 205 K*
Met-8 Band 9 (10.8 µm)	206.0
Met-11 Band 9 (10.8 µm)	205.9
GOES-16 Band 14 (11.2 µm)	206.1
Him-08 Band 13 (10.8 µm)	206.8
FY2G Band 2 (10.8 µm)	203.5
COMS Band 4 (10.8 µm)	206.7

2.3 Angular transformation

Differences in viewing and solar geometry will lead to inconsistent DCC responses between the reference VIIRS and the target GEO sensors. For direct inter-calibration using DCC-IT, it is essential to normalize both the sensors' DCC observations to a uniform set of angular

conditions. This angular transformation is performed using the Hu angular distribution model (ADM) [2] that normalizes each DCC pixels to an overhead-sun and nadir viewing configuration. Because DCC migrate seasonally with the sun [5], a lack of anisotropic correction may also results in a larger temporal variability in the DCC response. An anisotropy-corrected DCC pixel radiance is computed as follows:

$$L_{corrected} = \frac{L_{observed}}{d^2 \times \cos(SZA) \times R(SZA,VZA,RAA)} \quad \ldots\ldots\ldots\ldots\ldots\ldots\ldots\ldots (2)$$

where, $L_{observed}$ is the sensor-recorded DCC pixel radiance, d^2 is the Earth-sun distance correction factor, and R is the Hu ADM factor to scale $L_{observed}$ to overhead-sun and nadir viewing conditions. The Hu ADM look-up table and its reader can be downloaded from the following link. (Provide a website link to Hu ADM and reader)

If both VIIRS and GEO DCC pixel observations are in radiance units, Eq. 2 can be used to derive anisotropic-corrected DCC pixels for both sets of data. However, if the GEO imager DCC pixels are in sensor recorded digital counts, the following equation should be used for angular transformation of an observed DCC count ($Count_{observed}$) to anisotropy-corrected count ($Count_{corrected}$).

$$Count_{corrected} = \frac{Count_{observed} - SC}{d^2 \times \cos(SZA) \times R(SZA,VZA,RAA)} \quad \ldots\ldots\ldots\ldots\ldots\ldots\ldots\ldots (3)$$

where, *SC* is the space count of the GEO sensor. The *SC* must be subtracted from $Count_{observed}$ prior to angular transformation.

2.4 Statistical transformation of data

Unlike an invariant ground site-based calibration approach, for which the spatially averaged TOA reflectance over the site is regarded radiometrically and temporally stable over time, the DCC-IT is a large-ensemble statistical technique that relies on the assumption that the distribution of DCC reflectance in the visible spectrum remains constant in time. The anisotropy-corrected DCC pixel radiances, or $L_{corrected}$, are compiled into monthly probability distribution functions (PDFs). The modes of the monthly PDFs, which provide peak frequencies of DCC reflectance, are tracked over time to monitor the temporal radiometric stability of the sensor. While computing the PDFs, an optimization of the PDF bin size (Δ_{PDF}) is essential for deriving smooth PDFs. A smaller Δ_{PDF} can result in spiky PDFs with multiple peaks, whereas a larger Δ_{PDF} can provide smoother PDFs but the mode is less sensitive to small magnitude sensor drifts. A bin size of 0.2-0.4% of the average DCC mode radiance is recommended to derive robust monthly DCC PDFs and achieve optimal performance of the method.

Figure 3a and 3b show the monthly PDFs of GOES-16 ABI B2 (0.64 µm) before and after the anisotropic correction of the DCC pixels. Two sets of PDFs are seen in these plots that resulted from a change in the calibration algorithm of ABI. On April 23, 2019, the calibration of GOES-16 band 2 was adjusted by ~6.2% in the forward processing mode [11]. As a result, the PDFs are shifted towards left. It is evident from Figure 3a and 3b that the application of the Hu ADM results in more robust and consistent monthly PDFs. The Hu ADM is very effective in mitigating the angular dependencies of DCC reflectance in VIS-NIR bands. A previous study [4] showed a reduction in the natural variability of DCC response in VIS-NIR bands by up to ~60% using the Hu ADM. Similarly, Figure 3c shows that the monthly PDFs constructed from $L_{corrected}$ from the NOAA-20 VIIRS I1 band (0.64 µm). The VIIRS PDFs are consistent from month to month with their peaks (mode values) all lined up together as expected from a well-calibrated and stable

instrument. The so-computed VIIRS and GEO monthly PDF modes (radiances or counts) are later used for performing inter-calibration.

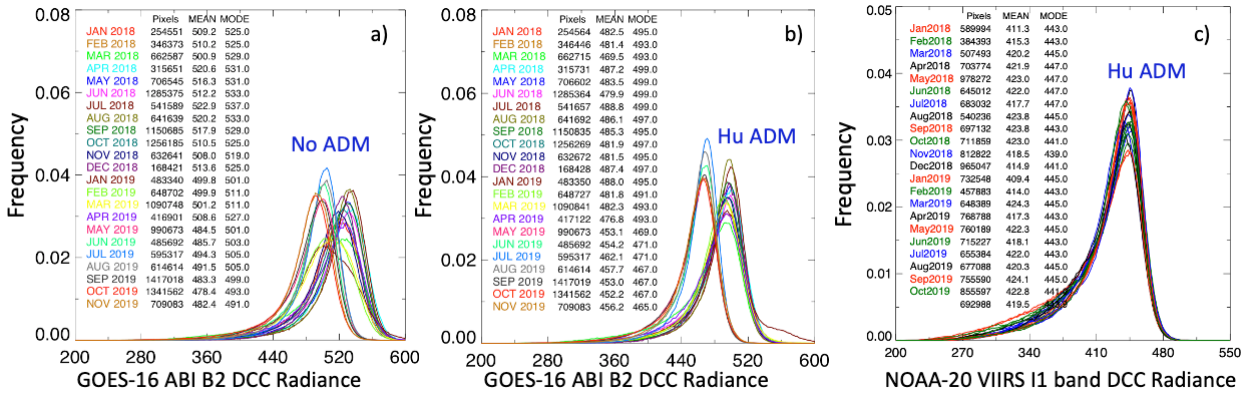

Figure 4: (a) The monthly DCC PDFs computed for GOES-16 ABI band 2. The PDFs are shifted left for May 2019 and onwards due to the adjustment in calibration on April 24, 2019. (b) Same as (a) but with anisotropic corrections applied to individual DCC pixels using the Hu ADM. (c) Same as (b) but for NOAA-20 VIIRS I1 band.

2.5 Seasonal correction

Certain GEO domains, such Meteosat 0E, exhibit greater intraannual variability in the DCC response that results in a noticeable seasonality in the DCC mode timeseries. Figure 5(a) shows a timeseries of the monthly DCC mode counts (red diamonds) computed for Meteosat-9 VIS band. The observed large natural variability in the DCC timeseries impairs the detection of smaller magnitude trends with statistical significance [6], [12], [13]. The month-to-month DCC response variability can be mitigated by utilizing an appropriate deseasonalization of the DCC monthly modes. This ATBD follows a ratio-to-moving-average method for deseasonalization of DCC mode timeseries as outlined by Bhatt et al. [13], [14]. This is performed in four steps.

1. A 12-month centered running mean is computed for each DCC mode values, except for the first five and last 6 entries, for which the 12-month centered running mean is not feasible to compute. Therefore, this approach of deseasonalization requires at least two full years of data.
2. A relative ratio between the actual month mode value and the 12-month centered running mean is determined.
3. A mean relative ratio or seasonal index (SI) is computed for each month by averaging the similar month relative ratios (mean of all January relative ratios, and so on). A monthly SI is a measure of how that particular-month DCC response compares with that of the average season.
4. Finally, the DCC modes are divided by month-specific SIs to yield seasonally adjusted time series.

The month-to-month seasonal variation (based on monthly SIs) in the Meteosat-1 VIS band DCC time series was found mostly within 2% as shown in Figure 5(b). The brightest and darkest DCC mode response over the 0E GEO domain was found for July and December months, respectively. The deseasonalization process resulted in a significant reduction (> 50%) of temporal standard error of the Meteosat-9 band 1 DCC time series, while preserving the temporal trend, as

shown in Figure 5(a). The lowered temporal variability reduces the uncertainty in the inter-calibration ratio as well as the estimation of the sensor trend.

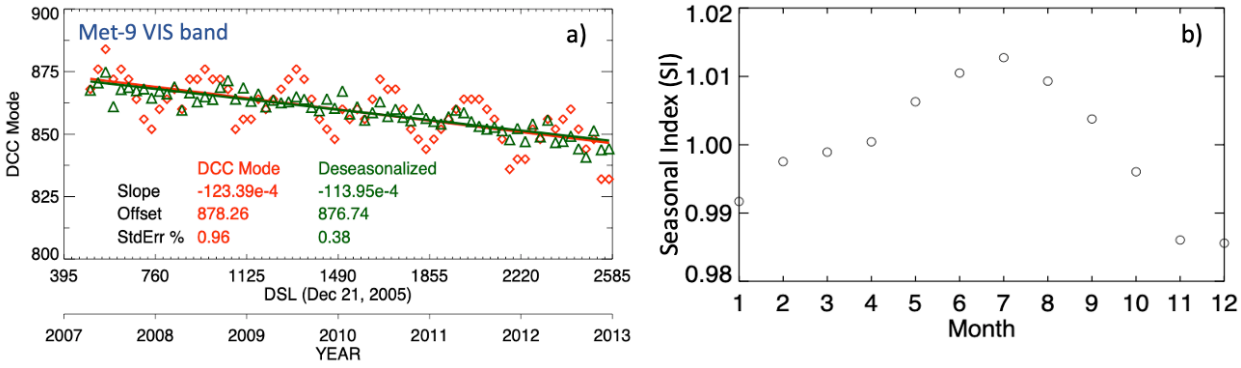

Figure 5: (a) Monthly DCC PDF mode timeseries for Meteosat-9 visible band before (red diamonds) and after (green triangles) deseasonalization performed using a ratio-to-moving-average method. (b) Monthly seasonal indices computed for Met-9 VIS band DCC monthly mode counts.

2.6 Reference DCC mode

The DCC-IT inter-calibration algorithm assumes that the nearly coincident and collocated, but not necessarily ray-matched, VIIRS and GEO DCC-mode reflectivity should be equal [1], [10]. To obtain the reference DCC-mode radiance ($L_{VIIRS,\ Mode}$) for a target GEO, the monthly DCC-mode radiances computed from the DCC pixels acquired over the specific GEO domain by the VIIRS imager are averaged. A standard deviation of the VIIRS monthly mode radiances is computed as 1-σ uncertainty in the reference mode radiance value. The DCC-mode MODIS radiance varies slightly by GEO domain as shown in Figure 6 for the VIIRS I1 band. The 0E GEO domain exhibits the largest DCC-mode radiance for VIS and NIR wavelengths.

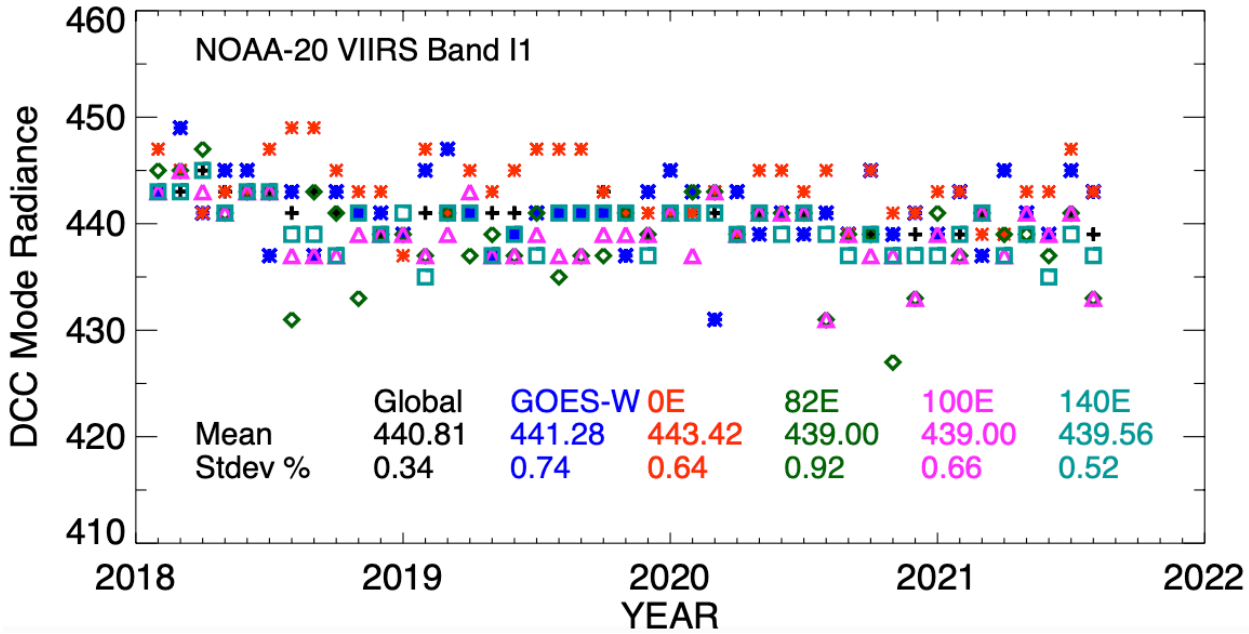

Figure 6: The monthly DCC modes derived from NOAA-20 VIIRS I1 band radiances organized by GEO domains.

The reference DCC mode radiances based on NOAA-20 VIIRS M3, M4, M5, M7, and I1 bands for prime GEO domains are listed in Table 2 along with the associated 1-σ uncertainty.

Table 2: Reference DCC mode values derived for different GEO domains using the NOAA-20 VIIRS VIS/NIR bands calibrated radiances.

NOAA-20 VIIRS Band	Global		GOES-W (e.g., GOES-15, 11)		GOES-E (e.g., GOES-12, 16)		0°E (e.g., Met-11, 10)		41°E (e.g., Met-8)		57°E (e.g., Met-7)	
	Mean	1-σ %	Mean	1-σ %	Mean	1-σ %	Mean	1-σ %	Mean	1-σ %	Mean	1-σ %
M3 (0.48 µm)	573.28	0.41	574.77	0.73	573.79	0.56	576.54	0.64	575.09	0.65	572.72	0.71
M4 (0.55 µm)	507.14	0.50	507.98	0.91	507.77	0.64	509.98	0.65	508.72	0.62	505.88	0.95
M5 (0.67 µm)	432.02	0.31	432.91	0.73	432.12	0.55	434.07	0.55	433.00	0.50	431.05	0.71
M7 (0.86 µm)	269.73	0.28	269.66	0.55	270.43	0.44	271.15	0.42	271.15	0.35	269.48	0.55
I1 (0.65 µm)	440.81	0.34	441.28	0.74	441.42	0.52	443.42	0.64	442.63	0.64	439.98	0.72

NOAA-20 VIIRS Band	82°E (e.g., INSAT-3D)		100°E (e.g., FY2G)		128°E (e.g., COMS)		140°E (e.g., MTSAT-2, Him-8)	
	Mean	1-σ %	Mean	1-σ %	Mean	1-σ %	Mean	1-σ %
M3 (0.48 µm)	571.19	0.84	571.00	0.69	571.14	0.75	571.28	0.59
M4 (0.55 µm)	505.14	0.95	504.86	0.84	505.19	0.89	506.16	0.69
M5 (0.67 µm)	430.12	0.85	430.44	0.54	430.63	0.63	430.81	0.51
M7 (0.86 µm)	268.76	0.51	268.94	0.41	269.06	0.50	269.15	0.49
I1 (0.65 µm)	439.00	0.92	439.00	0.66	439.47	0.66	439.56	0.52

2.7 Spectral band adjustment factor (SBAF)

The spectral band adjustment factor (SBAF) account for the non-shared spectral radiance differences between the reference VIIRS and target GEO imager bands caused by any disparity in their channel SRFs [15]–[17]. The SBAF is dependent on the Earth scene type used for inter-calibration. The DCC SBAF is derived from the SCanning Imaging Absorption spectroMeter for Atmospheric CHartographY (SCIAMACHY) level-1b version-7.03 hyperspectral footprint radiances using the NASA-Langley SCIAMACHY SBAF computation tool [16], [18]. Here's the link for the SBAF tool:
https://satcorps.larc.nasa.gov/cgi-bin/site/showdoc?mnemonic=SAT_CALIB_USER

Figure 7 shows the user interface of the SBAF tool. The procedure for computing the DCC SBAF for a given GEO imager referenced to NOAA-20 VIIRS is described below.

SBAF computation steps

1. Select "***Precise DCC***" from the Earth Spectra column
2. Select "***NOAA-20-VIIRS-V2F***" for **Reference (X-axis) SRF**
3. Select appropriate **Central Wavelength** for reference VIIRS SRF
4. Select target GEO imager for **Target (Y-axis) SRF**
5. Select appropriate **Central Wavelength** for target GEO SRF
6. Select "***Pseudo Radiance***" from the **Units** column for radiance SBAF
7. Select "***Force Fit***" for Regression analysis
8. Click the **Plot** button

The SRFs of GOES-16 ABI band 2 and NOAA-20 VIIRS I1 channel are shown in Figure 8(a). The two channels are mostly similar. The DCC SBAF regression output from the SBAF tool for this band pair is shown in Figure 8(b). The force-fit slope ($Slope_0$), which is the slope of linear regression forced through origin, provides the SBAF for spectral radiance corrections between the VIIRS and ABI channels. In this case, $\boldsymbol{L_{VIIRS,\ Mode}}$ must be multiplied by $Slope_0$=1.01 to derive the GOES-16 ABI band 2 DCC mode radiance referenced to the VIIRS I1 calibration.

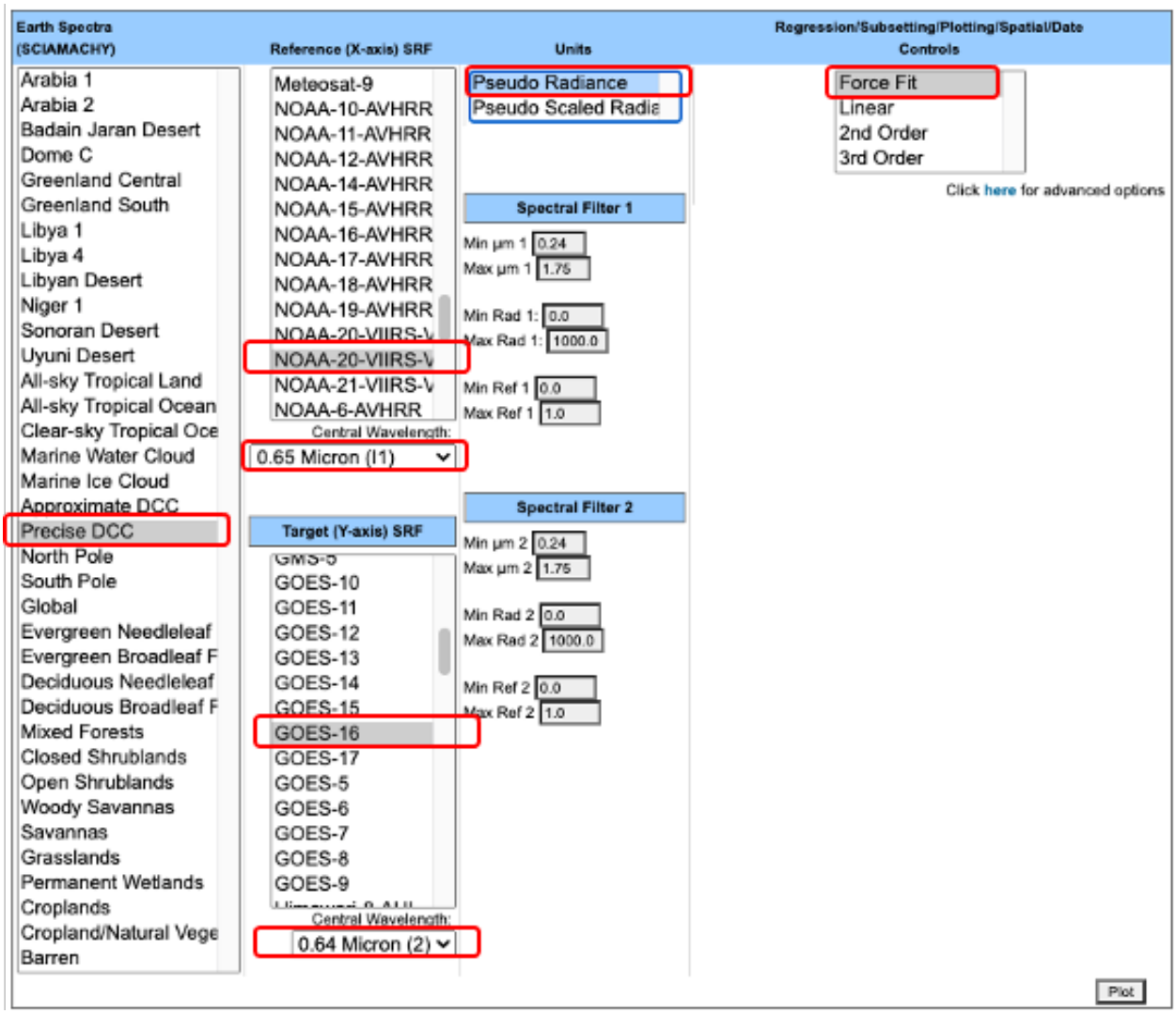

Figure 7: NASA Langley's SBAF computation tool interface and parameter settings.

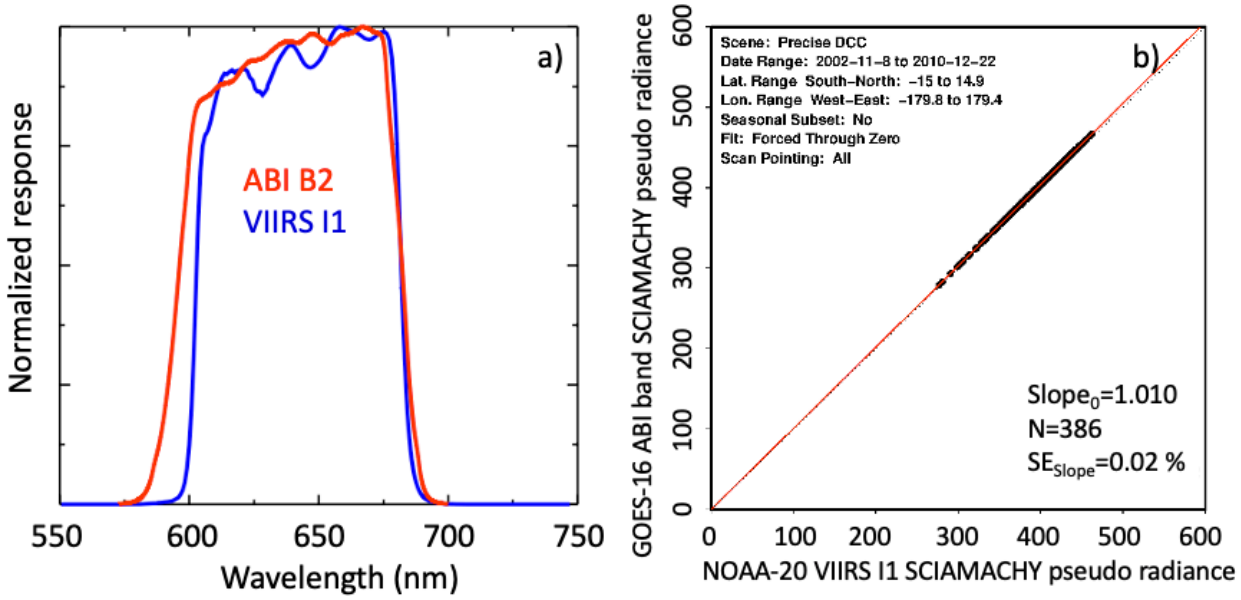

Figure 8: (a) SRFs of GOES-16 ABI band 2 and NOAA-20 VIIRS I1 channel. (b) SBAF regression of the NOAA-20 VIIRS I1 band and GOES-16 ABI band 2 SCIAMACHY footprint pseudo radiance ($Wm^{-2}sr^{-1}\mu m^{-1}$) pairs over DCC targets. $Slope_0$ provides the SBAF for spectral corrections between these two band pairs.

2.8 Computation of monthly calibration slope ($\gamma_{GEO,\,cal-slope}$)

The DCC-IT inter-calibration between the GEO and VIIRS sensors can be performed by comparing their monthly DCC mode responses. If the GEO DCC pixels are sensor-recorded counts, the inter-calibration can provide a monthly calibration slope ($\gamma_{GEO,\,cal-slope}$) to convert the GEO sensor counts to VIIRS-scaled radiances. The first step of computing $\gamma_{GEO,\,cal-slope}$ is to adjust the reference VIIRS DCC mode radiance ($L_{VIIRS,MODE}$) for spectral differences between the GEO/VIIRS band pair and compute the GEO equivalent reference mode radiance ($L_{GEO,MODE,reference}$). This can be done by multiplying $L_{VIIRS,MODE}$ by $Slope_0$, as described by Eq. 4.

$$L_{GEO,MODE,reference} = Slope_0 \times L_{VIIRS,MODE} \;\; (Wm^{-2}\mu m^{-1}sr^{-1}) \;\ldots\ldots\ldots\ldots(4)$$

$\gamma_{GEO,\,cal-slope}$ can be then computed by dividing $L_{GEO,MODE,reference}$ by the observed monthly GEO DCC mode count ($C_{GEO,MODE,observed}$), as shown in Eq. 5. It is noteworthy to mention that the space count must be subtracted from the GEO DCC pixel count prior to the computation of $C_{GEO,MODE,observed}$.

$$\gamma_{GEO,cal-slope} = \frac{L_{GEO,MODE,reference}}{C_{GEO,MODE,observed}} \; (Wm^{-2}\mu m^{-1}sr^{-1}/Count) \;\ldots\ldots\ldots (5)$$

$\gamma_{GEO,cal-slope}$ provides the radiometric gain to convert the GEO observed counts to spectral radiances for a given month. Any temporal radiometric drifting of the GEO sensor can be tracked from the timeseries of $\gamma_{GEO,cal-slope}$. Figure 9 shows the monthly $\gamma_{GEO,cal-slope}$ timeseries derived

for GOES-16 ABI band 2 using VIIRS M5 and I1 bands as reference. These two sets of $\gamma_{GEO,cal-slope}$ differ by ~0.8%, which is due to the absolute calibration difference between the VIIRS M5 and I1 bands. It is recommended to use an appropriate regression fit to characterize the $\gamma_{GEO,cal-slope}$ timeseries trend and estimate the temporal calibration slope of the GEO imager at any specific time using the fit.

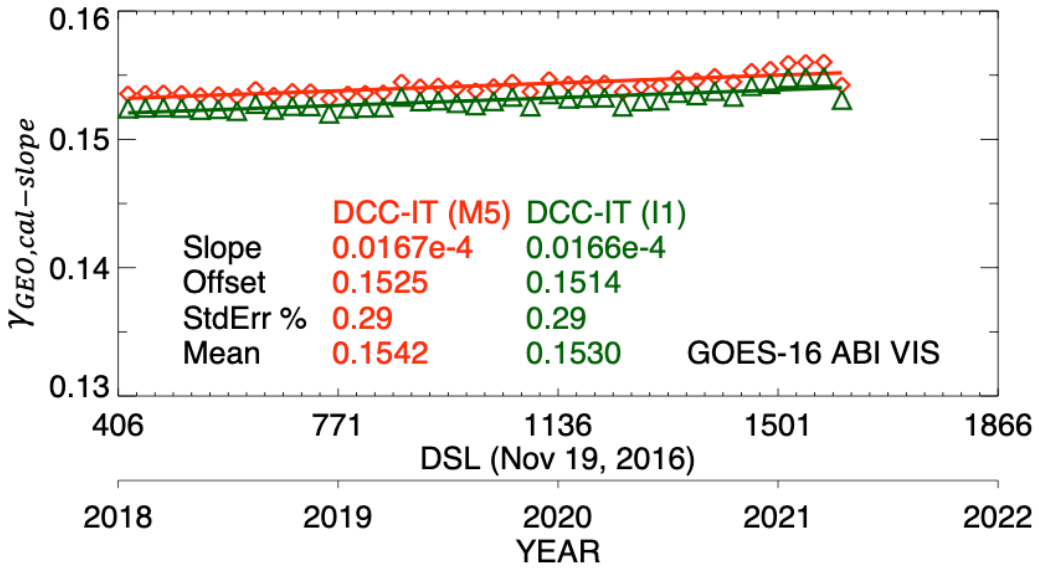

Figure 9: Calibration slope of GOES-16 ABI band 2 referenced to NOAA-20 VIIRS I1 calibration using ATO-RM and DCC-IT methods.

2.9 Computation of cross-calibration ratio ($\gamma_{cross-cal}$)

DCC-IT can also be used to compute a cross-calibration ratio, $\gamma_{cal-ratio}$, between two calibrated radiance (or reflectance) datasets. The $\gamma_{cal-ratio}$ between a target GEO and the reference VIIRS instruments can be computed using the following equation.

$$\gamma_{cal-ratio} = \frac{L_{GEO,MODE,reference}}{L_{GEO,MODE,observed}} \text{ (unitless)} \quad \ldots\ldots\ldots\ldots\ldots\ldots\ldots\ldots (6)$$

where $L_{GEO,MODE,reference}$ is the reference GEO DCC mode radiance based on VIIRS measurements (Eq. 4) and $L_{GEO,MODE,observed}$ is the observed monthly DCC PDF mode using the GEO L1B radiance dataset. $\gamma_{cal-ratio}$ provides the radiometric scaling factor or bias between the GEO and VIIRS imagers calibration.

2.10 Detection of GEO imager temporal trend

For detecting the relative temporal trend of the GEO imager, the reference VIIRS DCC measurements are not needed. As the sensor responsivity degrades over time, the peak or mode of the monthly DCC PDF shifts towards left. As such, the timeseries of $C_{GEO,MODE,observed}$ is adequate to reveal any temporal radiometric trend of the GEO sensor. For example, Figure 10 displays the monthly DCC Mode count derived for Meteosat-7 VIS band plotted over time. This example shows the PDF mode values are computed at two different Δ_{PDF}: 0.5 count (0.25% of the

mode count at the beginning of the record) and 2 count (1% of the mode count at the beginning of the record). While both timeseries can capture the long-term sensor degradation, the mode values computed at lower Δ_{PDF} is more sensitive to sensor responsivity change and can detect the gradual degradation. In addition, the temporal radiometric trending of the GEO sensor is also revealed by timeseries of $\gamma_{cal-ratio}$ and $\gamma_{GEO,cal-slope}$.

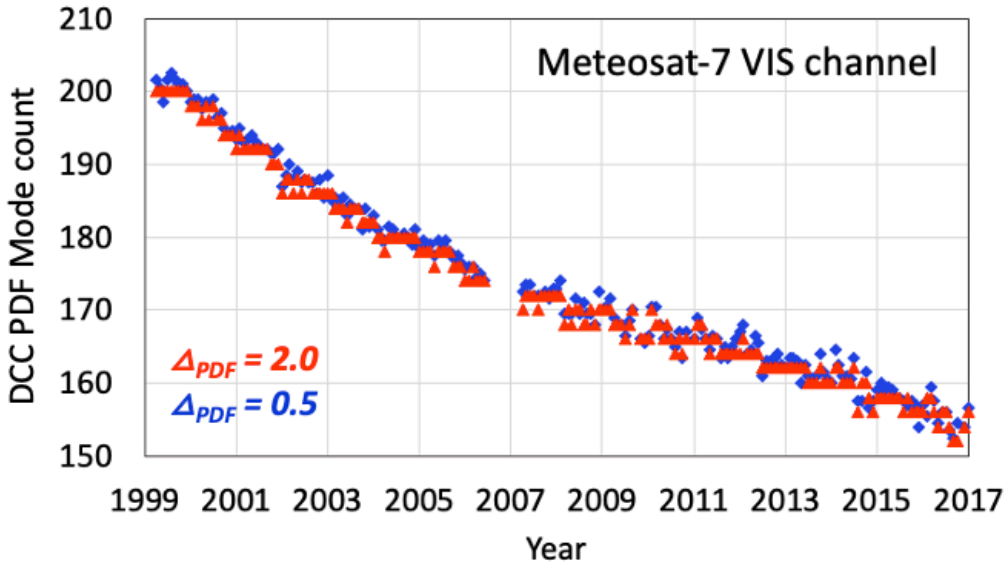

Figure 10: Temporal radiometric trend of Meteosat-7 VIS band based on the timeseries of $C_{GEO,MODE,observed}$ computed at two different PDF bin sizes.

2.11 Uncertainty analysis

Three prime sources of uncertainty are identified in the DCC-IT based GEO-VIIRS inter-calibration: uncertainty in the reference mode value computed from VIIRS DCC measurements (U_{Ref}), SBAF uncertainty (U_{SBAF}), and temporal regression uncertainty (U_{RegFit}). U_{Ref} is computed as the temporal standard deviation (1σ $uncertainty$) of the VIIRS monthly DCC mode radiances over a given GEO domain. These values are provided in Table 2. U_{SBAF} is the standard error of the SBAF regression slope and is directly provided by NASA Langley's SBAF computation tool. The ATBD implements a regression fit to the GEO DCC timeseries for estimating a time-dependent calibration slope. As such, the regression uncertainty must also be considered. U_{RegFit} is estimated as the standard error of the temporal regression. Total inter-calibration uncertainty is computed by summing these three uncertainty values in quadrature. The net DCC-IT inter-calibration uncertainty for GOES-16 ABI band 2 and VIIRS I1 channel is computed to be ~0.9%. Other sources of uncertainty could be from BT normalization, SCIAMACHY relative calibration inconsistency between channels, SRF changes in orbit, etc, the magnitudes of which are believed to be minimal compared to the three prime sources of uncertainty discussed above.

2.12 Flowchart of DCC-IT calibration procedure

Figure 11 shows a flowchart summarizing the procedure of processing the VIIRS DCC pixels for computing the reference DCC mode values over specific GEO domains. The flowchart for computing the GEO calibration slope using DCC-IT is shown in Figure 12.

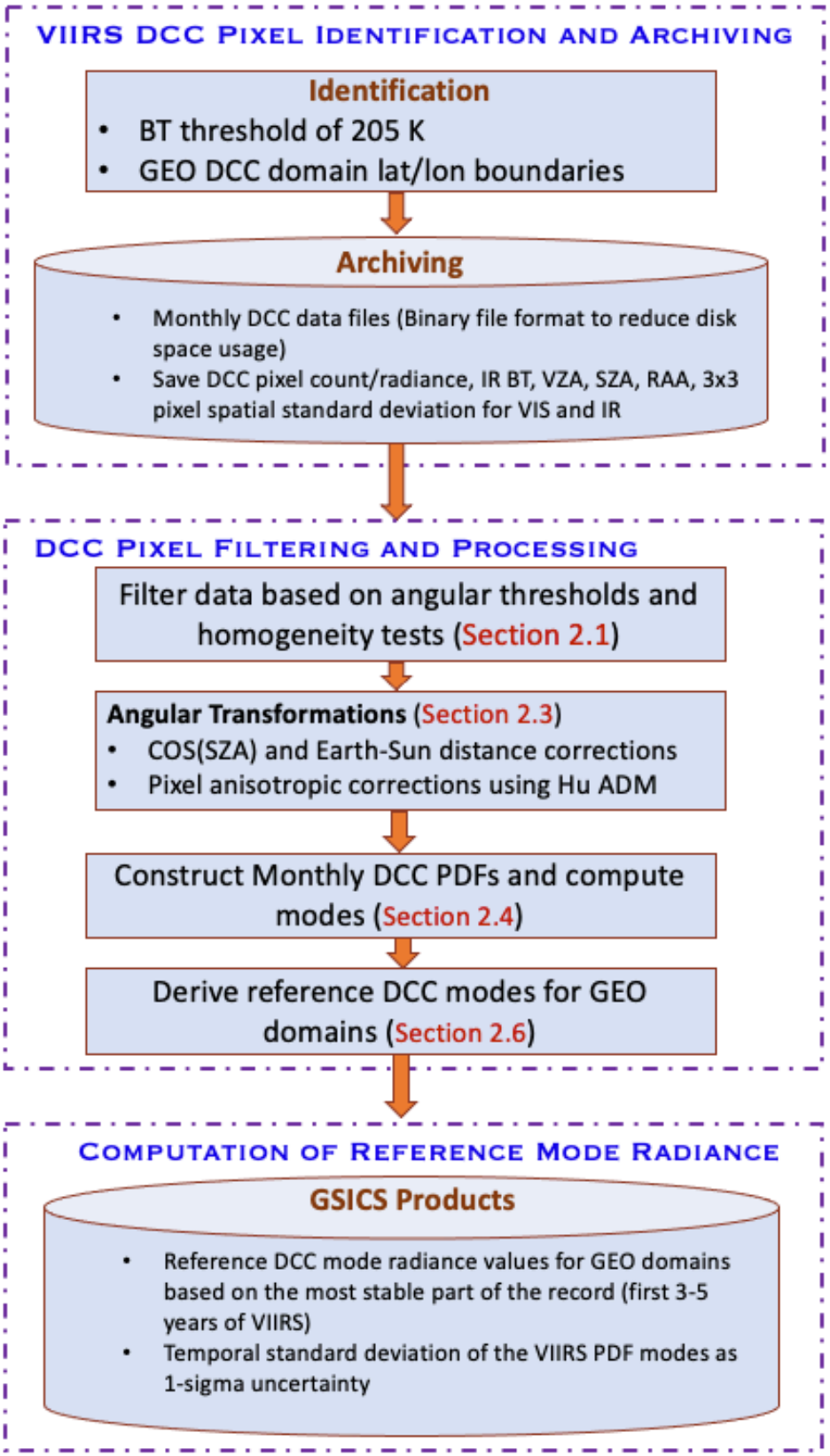

Figure 11: Flowchart showing the processing of DCC pixels for the reference VIIRS instrument and computation of the reference DCC mode.

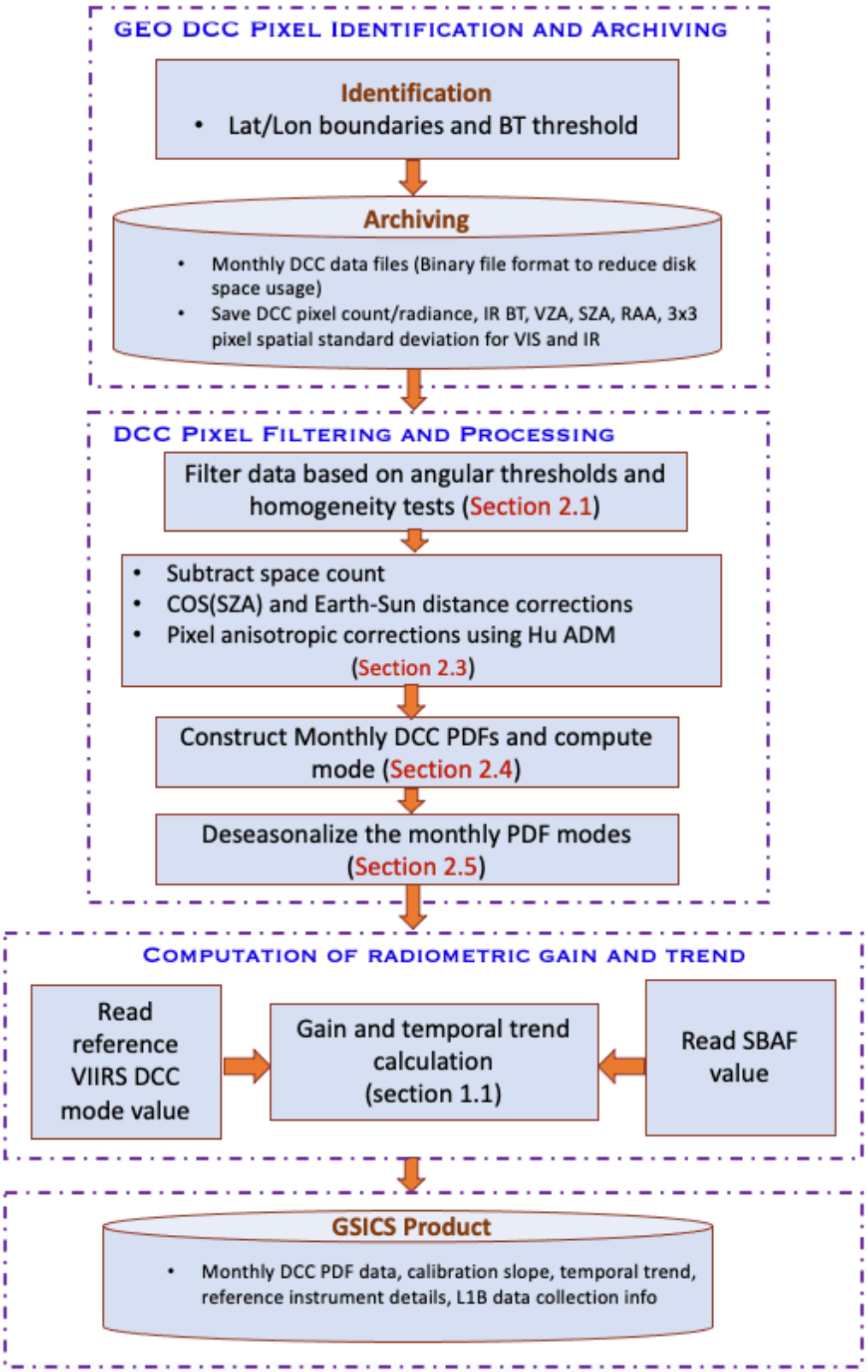

Figure 12: Flowchart showing the procedure for computing the calibration slope and temporal trend for a GEO visible channel using the DCC method.

3. GSICS Products

Will be discussed at the GSICS monthly meeting.

3.1 Purpose

3.2 Datasets

- NetCDF files containing VIIRS-based reference mode radiances and uncertainty values for GEO domains.
- Test datasets for GEO DCC samples, PDF, bin size, mode and mean, etc.

4. Limitations and future work

The DCC-IT calibration method described above is an attractive alternative to using ground invariant targets, as DCCs are significantly less impacted by water vapor absorption and offer high signal-to-noise ratio (SNR). For VIS and NIR solar spectrum, DCCs are nearly Lambertian, thereby offering robust inter-calibration between two imagers than any other earth invariant target. However, at SWIR wavelengths (>1 μm), the DCC reflectivity is highly dependent on wavelengths, ice particle size, BRDF, and IR BT threshold [13], [19]. Consequently, the DCC response shows large seasonal cycles (2%–3%) that diminish inter-calibration accuracy and the detection of trend. Also, the Hu ADM was also found ineffective for anisotropic corrections of DCC pixels at SWIR bands [13], [20]. The VIS-NIR DCC-IT method, therefore, must be revised to separate sensor calibration drifts and reflectivity variations in SWIR bands due to optical depth, particle size, and above-cloud water vapor variations. Bhatt et al. [6], [13] showed that the SWIR bands' DCC reflectance variability can be better characterized using wavelength-specific seasonal BRDFs. The application of these BRDF models was shown to effectively reduce the DCC temporal variability by up to 65% [4]. In future, we intend to provide a dedicated ATBD based on seasonal characterization of DCC reflectivity using well-calibrated LEO and GEO imager DCC measurements for extending the use of DCC-IT for calibrating SWIR channels.

5. References

[1] D. Doelling, C. Haney, R. Bhatt, B. Scarino, and A. Gopalan, "Geostationary visible imager calibration for the CERES SYN1deg edition 4 product," *Remote Sens.*, vol. 10, no. 2, 2018.

[2] Y. Hu, B. A. Wielicki, P. Yang, P. W. Stackhouse, B. Lin, and D. F. Young, "Application of deep convective cloud albedo observation to satellite-based study of the terrestrial atmosphere: Monitoring the stability of spaceborne measurements and assessing absorption anomaly," *IEEE Trans. Geosci. Remote Sens.*, vol. 42, no. 11, pp. 2594–2599, 2004.

[3] D. R. Doelling, L. Nguyen, and P. Minnis, "On the use of deep convective clouds to calibrate AVHRR data," in *Earth Observing Systems IX*, 2004, vol. 5542, p. 281.

[4] R. Bhatt, D. R. Doelling, B. R. Scarino, A. Gopalan, and C. O. Haney, "Advances in utilizing tropical deep convective clouds as a stable target for on-orbit calibration of satellite imager reflective solar bands," 2019, p. 53.

[5] D. R. Doelling, D. Morstad, B. R. Scarino, R. Bhatt, and A. Gopalan, "The characterization of deep convective clouds as an invariant calibration target and as a

visible calibration technique," *IEEE Trans. Geosci. Remote Sens.*, vol. 51, no. 3, pp. 1147–1159, 2013.
[6] R. Bhatt *et al.*, "Response Versus Scan-Angle Assessment of MODIS Reflective Solar Bands in Collection 6.1 Calibration," *IEEE Trans. Geosci. Remote Sens.*, vol. 58, no. 4, pp. 2276–2289, 2020.
[7] D. R. Doelling *et al.*, "A consistent AVHRR visible calibration record based on multiple methods applicable for the NOAA degrading orbits. Part II: Validation," *J. Atmos. Ocean. Technol.*, vol. 33, no. 11, pp. 2517–2534, 2016.
[8] R. Bhatt *et al.*, "A Consistent AVHRR Visible Calibration Record Based on Multiple Methods Applicable for the NOAA Degrading Orbits. Part I: Methodology," *J. Atmos. Ocean. Technol.*, vol. 33, no. 11, pp. 2499–2515, Sep. 2016.
[9] R. Bhatt *et al.*, "Initial stability assessment of S-NPP VIIRS reflective solar band calibration using invariant desert and deep convective cloud targets," *Remote Sens.*, vol. 6, no. 4, pp. 2809–2826, 2014.
[10] R. Bhatt, D. R. Doelling, C. Haney, D. A. Spangenberg, B. Scarino, and A. Gopalan, "Clouds and the Earth's Radiant Energy System strategy for intercalibrating the new-generation geostationary visible imagers," *J. Appl. Remote Sens.*, vol. 14, no. 03, p. 1, 2020.
[11] "GOES-ABI Calibration Event Log," 2020. [Online]. Available: https://www.star.nesdis.noaa.gov/GOESCal/goes_SatelliteAnomalies.php. [Accessed: 28-Feb-2020].
[12] E. C. Weatherhead *et al.*, "Factors affecting the detection of trends: Statistical considerations and applications to environmental data," *J. Geophys. Res. Atmos.*, vol. 103, no. D14, pp. 17149–17161, 1998.
[13] R. Bhatt, D. R. Doelling, B. Scarino, C. Haney, and A. Gopalan, "Development of seasonal BRDF models to extend the use of deep convective clouds as invariant targets for satellite SWIR-band calibration," *Remote Sens.*, vol. 9, no. 10, 2017.
[14] R. Bhatt *et al.*, "Characterizing response versus scan-angle for MODIS reflective solar bands using deep convective clouds," *J. Appl. Remote Sens.*, vol. 11, no. 1, p. 016014, 2017.
[15] P. M. Teillet, G. Fedosejevs, K. J. Thome, and J. L. Barker, "Impacts of spectral band difference effects on radiometric cross-calibration between satellite sensors in the solar-reflective spectral domain," *Remote Sens. Environ.*, vol. 110, no. 3, 2007.
[16] B. R. Scarino *et al.*, "A Web-Based Tool for Calculating Spectral Band Difference Adjustment Factors Derived from SCIAMACHY Hyperspectral Data," *IEEE Trans. Geosci. Remote Sens.*, vol. 54, no. 5, pp. 2529–2542, 2016.
[17] B. Scarino *et al.*, "Using SCIAMACHY to improve corrections for spectral band differences when transferring calibration between visible sensors," in *Earth Observing Systems XVII*, 2013, vol. 8510, p. 85100Q.
[18] "SCIAMACHY SBAF Tool." [Online]. Available: https://satcorps.larc.nasa.gov/cgi-bin/site/showdoc?mnemonic=SBAF. [Accessed: 28-Aug-2021].
[19] S. Platnick, J. Y. Li, M. D. King, H. Gerber, and P. V. Hobbs, "A solar reflectance method for retrieving the optical thickness and droplet size of liquid water clouds over snow and ice surfaces," *J. Geophys. Res. Atmos.*, vol. 106, no. D14, pp. 15185–15199, 2001.
[20] Q. Mu *et al.*, "Optimization of a deep convective cloud technique in evaluating the long-term radiometric stability of MODIS reflective solar bands," *Remote Sens.*, vol. 9, no. 6,

2017.